Tasmania
DEPARTMENT of INFRASTRUCTURE, ENERGY and RESOURCES

Mineral Resources Tasmania
Tasmanian Geological Survey
Record 2005/06

New whole-rock geochemical analyses of the Middle Cambrian Thomas Creek intrusive complex and associated lavas of the Noddy Creek Volcanics, western Tasmania

R. Reid, M. P. McClenaghan and D. B. Seymour

Abstract

Geochemical analyses (major and trace elements) of volcanic and igneous intrusive rocks from the Thomas Creek intrusive complex and its surrounds show that the rocks are a comagmatic suite of andesite and rhyodacite-dacite, correlating with previously recognised suites I and III of the Mt Read Volcanics. Pearce Element Ratio (PER) analysis indicates a primary geochemical variation due to igneous fractionation of clinopyroxene and plagioclase, with clinopyroxene crystallisation dominant early in the process. Hydrothermal alteration effects involved formation of K-feldspar, muscovite and chlorite, with associated loss of Na and Ca and gain of K. Separate but parallel K enrichment trends suggest that K metasomatism occurred in two phases, affecting rocks at different stages of fractionation. A possible explanation for this is a link between alteration (and mineralisation) and periodic pressure release at the top of the intrusion.

Introduction

The primary purpose of the study reported here was to carry out whole-rock major and trace-element geochemical analyses of a suite of previously unanalysed samples from the Thomas Creek intrusive complex and the adjacent andesitic lava sequence, and present the new results together with previous analyses (Table 1). Some first-pass interpretation of the geochemistry is presented. However, placing the new geochemistry in the context of a detailed paragenetic and alteration study (similar to that of Reid, 2001) is beyond the scope of this report. The new analyses were based on existing samples lodged in the Mineral Resources Tasmania rock/core store, and had two main sources:

- Diamond-drill core from the more recent phases of company mineral exploration of the Thomas Creek prospect (these samples are all from the intrusive complex);
- Surface rock samples collected in the late 1980s during the then Tasmania Department of Mines, Point Hibbs 1:50 000 scale geological mapping project (these samples are largely from the andesitic lava sequence, but include two samples of diorite from the intrusive complex).

Representative photomicrographs of the analysed samples are shown in Figure 1.

Geological setting

The Thomas Creek intrusive complex is a component of the Noddy Creek Volcanics, a 50 km long north-south belt of intermediate to acid volcanic, volcaniclastic and intrusive rocks which extends somewhat discontinuously from just south of Asbestos Point on the southern shore of Macquarie Harbour, to south of High Rocky Point on the southwest coast (Brown, 1988; Brown *et al.*, 1991; McClenaghan and Findlay, 1993). The most volumetrically significant components are in the northern 20 km of the belt (fig. 2). The Noddy Creek Volcanics belt lies some 10–15 km west of the main axis of the economically important Middle Cambrian Mount Read Volcanics belt, but is believed to be related to it. This is based on major and trace element geochemistry (McClenaghan and Findlay, 1993) and a U-Pb SHRIMP radiometric age of 502.8 ± 4.4 Ma (middle Middle Cambrian) obtained from igneous zircon in a felsic intrusive rock in the Timbertops area (fig. 2) (Black *et al.*, 1997).

The main focus of this report is the study of an oval-shaped dioritic intrusive complex (the Thomas Creek intrusive complex) which occurs near the southern end of the area of more substantial units in

the northern part of the volcanic belt (fig. 2, 3). Map relationships (which are not yet precisely established) indicate that the Thomas Creek complex intrudes andesitic lavas and associated volcaniclastic rocks of the Noddy Creek Volcanics, and an adjacent Cambrian lithicwacke-siltstone-conglomerate sequence which may stratigraphically underlie the andesites (fig. 3). The mineral prospectivity of the Noddy Creek Volcanics has been considerably enhanced by the discovery of intrusion-related Cu-Au mineralisation at the Thomas Creek prospect, which lies within the Thomas Creek intrusive complex (fig. 4). According to Reid (2001), the mineralisation and associated alteration show similarities to SW Pacific porphyry Cu-Au deposits, but with differences in alteration style and mineral components.

Reid (2001) found that copper mineralisation at Thomas Creek is hosted by intrusive diorite and feldspar-augite porphyritic andesite, which have been intruded by chalcopyrite-bearing porphyritic micromonzodiorite. Geochemistry indicated that the diorite and porphyritic micromonzodiorite form a co-magmatic fractionation series. Four stages of mineralisation were recognised:

1. Early magnetite and feldspar(albite)-silicate alteration.
2. Emplacement of Cu-bearing micromonzodiorite intrusions and precipitation of coeval actinolite and tourmaline veins.
3. K-feldspar–smectite vein formation.
4. Epidote and carbonate veining.

According to Reid (2001), phases 1 and 2 represent periods of magma emplacement with some mixing of magmatic-hydrothermal water with seawater-derived fluid; phase 3 veins appear to be of magmatic character, with minimal seawater influence; phase 4 probably represents final incursion of seawater-derived fluids as the magmatic system waned. Reid suggested that the mineralisation represents the root zone of a Mt Lyell-type hydrothermal system. Similarities were also noted with the alkaline porphyry Cu-Au deposits of British Columbia, with Thomas Creek possibly being the submarine analogue of a porphyry system formed in a back-arc environment.

Geochemistry

The Thomas Creek rocks can be geochemically classified as andesite and rhyodacite-dacite (fig. 5) based on a diagram using immobile or less mobile element ratios (Nb/Y vs Zr/TiO_2) devised by Winchester and Floyd (1977). The data show a coherent pattern of variation on this diagram, supporting the view that they represent a comagmatic suite.

The Thomas Creek rocks can be compared geochemically with Mount Read Volcanic (MRV) rocks using suites defined by Crawford *et al*. (1992). The samples plot in a coherent trend stretching across the fields for suites I, III, IV and V on a SiO_2 vs P_2O_5/TiO_2 diagram (fig. 6). On a SiO_2 vs Ti/Zr diagram (fig. 7), the trend ranges across the fields for suites I, II and III. The fields for suites I and III are common to these two diagrams, suggesting that the Thomas Creek rocks are similar to MRV suite I and III rocks. Suite I consists of lavas and shallow intrusive rocks and includes Eastern sequence felsic rocks, Central Volcanic Complex andesites and rhyolites, Tyndall Group dacites and rhyolites, quartz-feldspar porphyries mainly along the western side of the MRV, and the Darwin and Murchison granitoids (Crawford *et al*., 1992). Suite III includes basaltic and andesitic lavas from the Lynch Creek basalts and shallow intrusive rocks in the Howard Plains area (both part of the Western Volcano-sedimentary Sequence), and the hanging wall sequence of the Que-Hellyer Volcanics (Mt Charter Group; Crawford *et al*., 1992).

The Pearce Element Ratio (PER) analysis technique (Russell and Stanley, 1990) has been applied to the new set of geochemical analyses from the Thomas Creek area, in order to distinguish between chemical variation due to igneous fractionation and that due to hydrothermal alteration.

The first requirement of the technique is that the samples must be related to a common parent system that at one time was homogeneous, i.e. they are cogenetic. In this case this is assumed to be true, as the samples are from the Thomas Creek intrusive complex and the adjacent andesitic lava sequence, which are believed to be genetically related and display broadly coherent trends on geochemical plots.

The second requirement is to identify an element that did not participate in the material transfer process which produced the geochemical variation. This is termed a conserved element and can be used as a standardising denominator of the PERs. The least mobile elements that are not involved in likely fractionating minerals are the best possibilities for conserved elements. If two elements are plotted against each other and lie on a line that passes through the origin then they are likely to be conserved elements (Stanley and Madeisky, 1993). The Zr-Nb plot (fig. 8) comes closest to this condition, with $r = 0.666$ and the best fit line passing close to the origin but intersecting the Zr axis at a Zr value of 4.2 ppm. This suggests that Zr is slightly less well conserved than Nb, based on inequality analysis of the functional controls of slopes and intercepts on scatterplots (Stanley and Madeisky, 1993). However, the concentration of Nb is low in these samples, and thus relatively close to its detection limit (3 ppm). Because Zr concentrations are far higher and thus well above the Zr detection limit of 5 ppm, Zr will have low relative measurement error, and for that reason it has been preferred as the conserved element denominator.

Compositional variation in the samples is likely to be due to the net effect of igneous fractionation and hydrothermal alteration. The first task is to separate the least altered and more altered samples.

Geochemical variation in the least-altered samples should be dominantly due to igneous fractionation, which in this case is most likely to be plagioclase and clinopyroxene fractionation, as the rocks contain phenocrysts of those minerals. For the more altered samples the variation should indicate the character of the hydrothermal alteration.

A plot of Al/Zr molar vs (2Ca+Na)/Zr molar (fig. 9) is used to determine whether some of the compositional variation is consistent with plagioclase and/or clinopyroxene fractionation. Many of the samples plot on or close to the line of unit slope, consistent with plagioclase fractionation, and some others show a linear trend at greater slope, consistent with a combination of plagioclase and clinopyroxene fractionation. The remaining samples lie below the plagioclase control line and trend to lower (2Ca+Na)/Zr and higher Al/Zr molar values. The variation in these samples is consistent with Ca and Na metasomatic loss and addition of muscovite and chlorite, i.e. hydrothermal alteration. Samples plotting close to the plagioclase control line and above it are likely to be the least hydrothermally altered, and are distinguished from the others on the basis of their position on this diagram (samples with ((2Ca+Na)/Zr)/(Al/Zr) molar ratio > 0.85).

It might be considered that addition of Ca-bearing carbonate minerals in veins could cause some of the samples to plot above the plagioclase control line, despite being considerably hydrothermally altered. Unfortunately CO_2 was analysed for only 33 of the 61 samples considered in this study, so a full assessment of the importance of carbonate minerals in controlling the compositional variation is not possible. Of the 33 samples analysed for CO_2, only three had CO_2 values greater than 0.25%, and so the impact of Ca-carbonate minerals on the chemical variation is likely to have been small.

A further two diagrams support plagioclase and clinopyroxene as the likely fractionating phases for the least hydrothermally altered samples. A plot of (Al-2Ca)/Zr molar vs Na/Zr molar (fig. 10) shows that most of the least hydrothermally altered samples lie along a line of unit slope, consistent with variation due to albite fractionation. Some of the more CaO-rich samples have negative (Al-2Ca)/Zr molar values and do not plot on this diagram. These samples belong to the early part of the fractionation trend which was dominated by clinopyroxene fractionation. As clinopyroxene was removed from the melt the (Al-2Ca)/Zr molar values became positive and plagioclase became a more significant fractionation phase. The more altered samples plot below the unit-slope line with a horizontal trend, consistent with Ca-bearing minerals being replaced by chlorite and muscovite. On a plot of (Al/2-Na/2)/Zr molar vs Ca/Zr molar (fig. 11), the least hydrothermally altered samples form a linear trend with a slope greater than unity, consistent with a combination of anorthite and clinopyroxene fractionation. Again the more altered samples have a poorly defined horizontal trend, consistent with muscovite and chlorite formation but also consistent with Na and Ca metasomatic loss.

A plot of (Ca-Al/2+Na/2)/Zr molar versus (Al/2-Na/2)/Zr molar (fig. 12) shows different poorly defined trends for the least and more hydrothermally altered samples. The least altered samples plot on a trend with a slope intermediate between the anorthite control line (vertical) and the clinopyroxene control line (horizontal), consistent with a combination of plagioclase and clinopyroxene fractionation. The more altered samples define a trend with a slope of about -1, parallel with the control by orthoclase, muscovite and chlorite.

The nature of the variation can be further tested with a plot of Al/Zr molar vs K/Zr molar (fig. 13). On this diagram the least altered samples define a trend of low slope (~0.15), lying between the control line for chlorite and plagioclase and the control line for muscovite. The deviation of the trend from the plagioclase control line (horizontal) suggests that there may be a minor effect from K metasomatic gain and/or growth of muscovite. Some of the more altered samples plot on a similar trend, but as their variation was not consistent with plagioclase fractionation on the previously described diagrams, their variation is more likely to have been caused by a combination of addition of chlorite and muscovite. The other more altered samples define two separate vertical trends consistent with K metasomatic gain. These separate but parallel trends suggest that the metasomatism affected rocks at different stages of the fractionation process, and may have happened in two phases.

In summary, the primary variation in these rocks was due to igneous fractionation of clinopyroxene and plagioclase, with clinopyroxene being dominant in the early part of the process. The variation caused by hydrothermal alteration was due to the formation of K-feldspar, muscovite and chlorite, and loss of Na and Ca and gain of K.

The alteration trends for the Thomas Creek area rocks may also be displayed (fig. 14) on the 'boxplot' diagram (Large, 1997) formed by plotting the Ishihawa alteration index (AI) against the chlorite-carbonate-pyrite index (CCPI). The diagram shows an unaltered box in the central part where less altered or unaltered rocks from the MRV generally plot. The less altered rocks, distinguished in this study (based on the PERs diagrams) for the Thomas Creek area, plot within the box forming a broad trend consistent with igneous fractionation. Some of the more altered samples plot with the less altered samples but most form two trends extending to higher AI and slightly lower CCPI values outside the box. The alteration trends are consistent with hydrothermal alteration as the altered samples generally plot above the calcite-sericite tie line which approximately separates alteration trends due to hydrothermal alteration above the line from those due to diagenetic alteration below the line (Allen *et al.*, 1998).

Conclusions

This study has shown that the Thomas Creek rocks can be geochemically classified as andesite and rhyodacite-dacite, and that they represent a comagmatic suite. Immobile element ratios indicate that they correlate geochemically with suites I and III of the Mt Read Volcanics, using the definitions of Crawford *et al*. (1992).

Pearce Element Ratio (PER) analysis applied to the Thomas Creek samples indicates a primary geochemical variation due to igneous fractionation of clinopyroxene and plagioclase, with clinopyroxene crystallisation dominant in the early part of the process.

PER analysis also indicates hydrothermal alteration effects, involving the formation of K-feldspar, muscovite and chlorite, and the loss of Na and Ca and gain of K. Separate but parallel alteration trends of K enrichment on some geochemical plots suggest that K metasomatism affected rocks at different stages of fractionation, and so may have occurred in two phases. One possible explanation is a link between alteration (and mineralisation) and periodic pressure release at the top of the intrusion.

Because this study is based only on overall geochemical trends in the analysed samples, it does not represent a test of the detailed paragenetic/mineralisation model of Reid (2001). The new geochemical data would provide a basis for further such detailed research.

Acknowledgements

Dr Jafar Taheri and Dr Geoff Green are thanked for reviewing the manuscript.

References

ALLEN, R. L.; GIFKINS, C. C.; LARGE, R. R.; HERRMANN, W. 1998. Discrimination of diagenetic, hydrothermal and metamorphic alteration. *Report AMIRA/ARC Project P439* 1:73–78.

BLACK, L. P.; SEYMOUR, D. B.; CORBETT, K. D.; COX, S. E.; STREIT, J. E.; BOTTRILL, R. S.; CALVER, C. R.; EVERARD, J. L.; GREEN, G. R.; MCCLENAGHAN, M. P.; PEMBERTON, J.; TAHERI, J.; TURNER, N. J. 1997. Dating Tasmania's oldest geological events. *Record Australian Geological Survey Organisation* 1997/15.

BROWN, A. V. 1988. *Geological Atlas 1:50 000 series. Sheet 78 (7912S). Montgomery*. Department of Mines Tasmania.

BROWN, A. V.; FINDLAY, R. H.; MCCLENAGHAN, M. P.; SEYMOUR, D. B. 1991. Synopsis of the regional geology of the Macquarie Harbour, Point Hibbs and Montgomery 1:50 000 map sheets. *Report Department of Resources and Energy Tasmania* 1991/21.

CORBETT, K. D. 2002. *Bedrock geological map of the Elliott Bay–Macquarie Harbour area, south-west Tasmania*. Mineral Resources Tasmania.

CRAWFORD, A. J.; CORBETT, K. D.; EVERARD, J. L. 1992. Geochemistry of the Cambrian volcanic-hosted massive sulphide-rich Mount Read Volcanics, Tasmania, and some tectonic implications. *Economic Geology* 87:597–619.

LARGE, R. R. 1997. The Hercules-Mt Read traverse: Relationships between volcanic mineralogy, alteration and geochemistry. *Report AMIRA/ARC Project P439* 3:153–233.

MCCLENAGHAN, M. P.; FINDLAY, R. H. 1993. Geological Atlas 1:50 000 series. Sheet 64 (7913S). Macquarie Harbour. *Explanatory Report Geological Survey Tasmania*.

REID, R. 2001. *Cambrian intrusion-related copper mineralisation at the Thomas Creek prospect, southwestern Tasmania*. M. Econ. Geology thesis, University of Tasmania, Hobart.

RUSSELL, J. K.; STANLEY, C. R. (ed.). 1990. Theory and application of Pearce Element Ratios to geochemical data analysis. *Short Course Notes Geological Association of Canada* 8.

SEYMOUR, D. B.; GREEN, D. 2001. *Digital Geological Atlas 1:25 000 scale series. Sheet 3628. Hibbs*. Mineral Resources Tasmania.

STANLEY, C. R.; MADEISKY, H. E. 1993. Pearce Element Ratio Analysis: Applications in lithogeochemical exploration. *Short Course Notes Mineral Deposit Research Unit, University of British Columbia* 8.

WINCHESTER, J. A.; FLOYD, P. A. 1977. Geochemical discrimination of different magma series and their differentiation products using immobile elements. *Chemical Geology* 20:325-343.

[2 November 2005]

Table 1

Compilation of whole-rock analyses of the Thomas Creek intrusive complex and associated lavas.

Sample No	R007901	R007902	R007903	R007904	R007905	R007906	R007907	R007908	R007909	R007910
Rock Code#	1	1	4	1	3	2	2	2	2	3
AMG mE	369800	369800	369800	369800	369800	369800	369800	369800	369800	370000
AMG mN	5285667	5285667	5285667	5285858	5285858	5285858	5285858	5285858	5285858	5285900
SiO_2	61.71	57.23	66.10	50.01	57.75	56.60	54.30	56.46	58.25	57.42
TiO_2	0.62	0.60	0.39	0.71	0.57	0.67	0.75	0.56	0.63	0.69
Al_2O_3	15.48	14.39	15.12	15.21	15.08	16.16	16.17	13.33	16.43	17.03
FeO*	5.47	10.65	4.57	10.45	8.67	7.35	9.54	9.10	7.67	6.18
Fe_2O_3	3.58	5.67	2.43	3.66	4.06	3.23	4.73	3.81	3.95	2.22
FeO	2.25	5.54	2.38	7.15	5.02	4.44	5.28	5.67	4.12	4.18
MnO	0.03	0.08	0.04	0.13	0.05	0.12	0.06	0.09	0.06	0.06
MgO	1.89	4.04	1.76	7.93	3.98	6.22	5.29	6.61	3.96	4.12
CaO	1.25	2.66	0.39	5.00	2.01	4.29	4.88	4.99	3.10	0.57
Na_2O	3.13	3.65	3.01	2.25	2.10	2.57	2.91	2.46	2.81	2.94
K_2O	6.50	2.76	6.45	2.77	5.95	1.77	2.38	1.95	2.39	6.81
P_2O_5	0.08	0.15	0.10	0.12	0.12	0.09	0.13	0.14	0.14	0.14
SO_3	0.12	0.08	0.03	0.04	0.10	0.13	0.04	0.06	0.11	0.10
CO_2	0.13	0.22	0.05	0.97	0.06	0.14	0.10	0.09	0.29	0.08
H_2O^+	2.60	2.49	1.49	3.81	2.76	3.52	2.97	3.20	3.27	3.03
S	1.1	0.1	0.0	0.0	0.1	0.1	0.0	0.1	0.1	0.2
TOTAL	99.37	99.57	99.71	99.75	99.61	99.93	99.98	99.44	99.52	99.39
LOI	2.48	2.10	1.27	3.98	2.26	3.17	2.49	2.66	3.11	2.65
Nd	-20	-20	30	-20	-20	-20	-20	-20	-20	-20
Ce	-28	-28	76	-28	-28	-28	-28	-28	-28	-28
La	27	-20	54	-20	-20	-20	-20	-20	-20	-20
Ba	180	370	1300	760	1250	340	320	450	540	1700
Cr	40	175	29	460	90	130	78	390	100	94
V	59	250	78	240	195	69	270	210	200	200
Sc	18	40	-9	36	25	40	36	34	23	21
Th	-10	19	21	20	17	13	15	23	15	17
Sr	140	200	76	195	155	270	270	280	270	125
U	-10	-10	11	-10	-10	-10	-10	-10	-10	-10
Rb	230	185	200	125	200	115	170	97	115	190
Y	18	24	32	26	27	11	20	30	20	27
Zr	175	170	145	105	170	135	125	185	180	170
Nb	5	6	10	5	8	6	5	8	7	8
Mo	6	8	-5	-5	-5	-5	6	-5	-5	-5
Co	80	21	11	24	26	37	19	27	24	33
As	21	-20	-20	-20	-20	-20	-20	-20	-20	-20
Bi	-5	-5	-5	-5	-5	-5	-5	-5	-5	-5
Ga	13	16	16	16	17	16	18	15	18	17
Zn	37	52	28	63	31	51	36	51	39	85
W	-10	-10	-10	-10	-10	-10	-10	-10	-10	-10
Cu	650	23	40	280	62	66	450	62	105	1000
Ni	88	49	21	180	39	40	41	66	27	97
Sn	-9	-9	-9	-9	-9	-9	-9	-9	-9	-9
Pb	-10	-10	-10	-10	-10	-10	-10	-10	-10	-10

Rock code 1 is feldspar-augite porphyritic andesite (minor clastic/breccia component)
Rock code 2 is medium-grained equigranular to weakly augite porphyritic diorite
Rock code 3 is porphyritic micromonzodioritic intrusions
Rock code 4 is acid (latite-?) andesite (quartz bearing)

Table 1

Compilation of whole-rock analyses of the Thomas Creek intrusive complex and associated lavas (continued).

Sample No	R007911	R007912	R007913	R007914	R007915	R007916	R007917	R007918	R007919	R007920
Rock Code#	3	1	3	1	1	1	1	1	1	2
AMG mE	370000	369600	369600	369600	369600	369600	369600	369600	369600	369600
AMG mN	5285900	5285750	5285750	5285750	5285750	5285925	5285925	5285925	5285815	5285815
SiO_2	51.61	56.24	56.78	60.64	53.12	55.16	58.75	55.56	50.35	58.24
TiO_2	0.69	0.65	0.57	0.72	0.64	0.74	0.62	0.70	0.65	0.55
Al_2O_3	16.89	16.69	14.27	16.38	15.12	19.96	17.31	18.59	15.43	14.99
FeO*	10.37	6.19	7.74	5.14	10.86	6.79	4.99	6.95	11.39	8.41
Fe_2O_3	5.16	1.72	3.24	1.69	4.49	3.33	1.40	3.50	5.86	4.97
FeO	5.73	4.64	4.83	3.61	6.82	3.80	3.73	3.80	6.12	3.93
MnO	0.08	0.07	0.08	0.05	0.12	0.04	0.11	0.10	0.07	0.10
MgO	5.24	6.02	6.34	3.74	6.42	3.56	6.05	4.42	6.28	3.54
CaO	4.00	3.91	5.40	3.23	3.91	5.00	2.50	4.89	5.92	4.71
Na_2O	3.78	5.07	4.33	4.68	3.31	3.04	3.76	3.11	3.62	3.72
K_2O	2.82	0.97	0.73	1.68	0.93	2.06	1.84	1.97	1.94	1.84
P_2O_5	0.12	0.03	0.04	0.04	0.10	0.13	0.10	0.15	0.13	0.14
SO_3	0.09	0.03	0.04	0.07	0.04	0.05	0.02	0.06	0.10	0.10
CO_2	0.07	0.22	0.11	0.08	1.21	0.15	0.03	0.09	0.07	0.06
H_2O^+	3.49	3.40	2.79	2.96	3.31	2.87	3.61	2.89	3.27	2.79
S	0.1	0.0	0.0	0.1	0.0	0.0	0.0	0.0	0.1	0.1
TOTAL	99.76	99.66	99.54	99.57	99.53	99.87	99.83	99.82	99.80	99.68
LOI	2.93	3.11	2.37	2.64	3.77	2.60	3.22	2.56	2.66	2.41
Nd	-20	-20	-20	-20	-20	-20	-20	-20	-20	-20
Ce	-28	-28	-28	-28	-28	-28	-28	-28	-28	-28
La	-20	-20	-20	-20	-20	-20	-20	-20	-20	-20
Ba	340	130	120	250	210	540	400	480	450	390
Cr	135	270	260	180	240	38	115	65	170	79
V	230	93	125	86	240	310	62	360	230	180
Sc	34	31	28	27	39	22	39	26	32	28
Th	20	18	20	13	17	16	12	98	19	18
Sr	250	110	190	115	210	340	310	280	155	125
U	-10	-10	-10	-10	-10	-10	-10	-10	-10	-10
Rb	155	40	39	60	65	135	105	120	86	57
Y	35	12	21	8	24	12	8	10	18	24
Zr	120	155	150	165	110	135	155	105	100	165
Nb	4	5	4	5	4	6	4	3	4	7
Mo	-5	-5	-5	5	-5	-5	-5	-5	-5	-5
Co	30	18	21	24	24	14	19	16	38	23
As	-20	-20	-20	-20	-20	-20	-20	-20	-20	-20
Bi	-5	-5	-5	-5	48	-5	-5	-5	-5	-5
Ga	18	18	16	16	18	20	16	18	17	16
Zn	80	50	45	52	56	27	31	34	55	34
W	-10	-10	-10	-10	-10	-10	-10	-10	-10	-10
Cu	20	61	290	57	1500	20	37	100	320	28
Ni	79	54	48	49	54	11	30	30	85	40
Sn	-9	-9	-9	-9	-9	-9	-9	-9	-9	-9
Pb	-10	-10	-10	-10	26	-10	-10	-10	-10	-10

Rock code 1 is feldspar-augite porphyritic andesite (minor clastic/breccia component)
Rock code 2 is medium-grained equigranular to weakly augite porphyritic diorite
Rock code 3 is porphyritic micromonzodioritic intrusions
Rock code 4 is acid (latite-?) andesite (quartz bearing)

Table 1

Compilation of whole-rock analyses of the Thomas Creek intrusive complex and associated lavas (continued).

Sample No	R007921	R001678	R002046	R002048	R002052	R002054	R002055	R002056	R002057	R002058
Rock Code#	1	1	1	1	1	4	1	1	2	2
AMG mE	369600	367280	367675	367770	367990	368060	368860	369005	369545	369630
AMG mN	5285815	5288980	5288845	5288815	5288630	5288530	5287780	5287765	5286900	5286670
SiO_2	57.77	50.58	57.33	51.16	63.21	60.48	53.25	58.08	52.62	59.42
TiO_2	0.65	0.43	0.79	0.52	0.59	0.65	0.52	0.57	0.49	0.56
Al_2O_3	15.05	10.51	13.80	15.17	14.87	17.50	13.41	13.30	13.31	13.74
FeO*	6.78	8.19	8.41	9.71	4.87	4.80	7.62	6.93	8.37	4.18
Fe_2O_3	3.09	2.74	2.41	3.71	2.55	2.39	3.25	3.62	4.14	1.71
FeO	3.99	5.73	6.24	6.37	2.58	2.64	4.70	3.67	4.64	2.64
MnO	0.09	0.18	0.25	0.40	0.18	0.15	0.25	0.18	0.07	0.09
MgO	4.93	12.18	4.69	6.66	2.67	2.25	7.75	5.30	8.77	5.87
CaO	5.90	10.61	4.79	8.05	4.35	2.22	8.59	7.71	8.86	9.38
Na_2O	3.96	1.22	2.94	4.30	4.82	4.74	3.75	4.34	3.21	3.57
K_2O	1.60	2.39	3.88	0.19	2.35	3.98	2.01	1.19	1.27	1.09
P_2O_5	0.03	0.08	0.18	0.13	0.10	0.09	0.11	0.11	0.13	0.03
SO_3	0.05	0.01	0.02	0.01	0.01	0.01	0.01	0.01	0.01	0.01
CO_2	0.19	0.03	0.24	0.13	0.18	0.02	0.19	0.03	0.06	0.03
H_2O^+	2.36	3.13	2.37	3.06	1.50	2.15	2.11	1.77	2.38	1.65
S	0.0	0.0	0.0	0.0	0.0	0.0	0.0	0.0	0.0	0.0
TOTAL	99.66	99.81	99.93	99.85	99.95	99.27	99.89	99.89	99.94	99.79
LOI	2.11	2.52	1.92	2.49	1.39	1.88	1.77	1.39	1.93	1.39
Nd	-20	100	40	28	-20	35	-20	20	32	-20
Ce	-28	105	69	47	38	76	-28	39	40	-28
La	-20	115	41	35	26	49	26	22	-20	-20
Ba	420	540	960	64	680	1260	520	220	300	170
Cr	175	950	84	360	43	10	370	230	380	260
V	110	220	230	220	110	150	220	185	280	91
Sc	34	43	24	31	14	13	33	23	36	26
Th	14	13	21	18	12	16	13	-10	15	13
Sr	230	200	190	330	230	310	280	260	310	300
U	-10	-10	-10	-10	-10	-10	-10	-10	-10	-10
Rb	71	95	135	6	89	145	73	36	52	45
Y	15	35	38	31	24	40	35	30	34	20
Zr	155	59	200	95	145	190	80	110	115	140
Nb	4		11	4	5	8		3	9	3
Mo	-5	-5	-5	-5	-5	-5	-5	-5	-5	-5
Co	21	52	37	41	12	18	35	24	28	14
As	-20	-20	23	-20	-20	-20	-20	-20	-20	-20
Bi	-5	-5	-5	-5	-5	-5	-5	-5	-5	-5
Ga	16	12	16	15	14	17	13	13	17	15
Zn	27	75	73	140	39	140	91	84	22	24
W	-10	-10	-10	-10	-10	-10	-10	-10	-10	-10
Cu	70	-5	-5	12	6	20	-5	-5	1070	18
Ni	27	270	25	155	38	33	175	51	145	55
Sn	-9	-9	-9	-9	-9	-9	-9	-9	-9	-9
Pb	-10	-10	-10	-10	-10	-10	-10	-10	32	-10

Rock code 1 is feldspar-augite porphyritic andesite (minor clastic/breccia component)
Rock code 2 is medium-grained equigranular to weakly augite porphyritic diorite
Rock code 3 is porphyritic micromonzodioritic intrusions
Rock code 4 is acid (latite-?) andesite (quartz bearing)

Table 1

Compilation of whole-rock analyses of the Thomas Creek intrusive complex and associated lavas (continued).

Sample No	R002059	R002060	R002062	18520	18521	18522	18523	18524	18525	18526
Rock Code#	4	1	4	1	2	2	4	2	4	1
AMG mE	369695	369463	369542	370000	370000	370000	369600	369600	369800	369800
AMG mN	5286505	5287595	5287500	5285900	5285900	5285900	5285750	5285815	5285667	5285858
SiO_2	55.09	61.06	71.91	52.95	51.38	55.94	56.06	60.54	65.7	55.74
TiO_2	0.80	0.55	0.19	0.77	0.73	0.56	0.66	0.59	0.36	0.56
Al_2O_3	16.66	13.76	13.79	15.91	17.43	13.68	16.24	16.34	15.11	13.41
FeO*	7.97	8.65	1.73	12.31	9.89	9.33	8.97	4.93	4.46	9.27
Fe_2O_3	4.63	5.67	1.63	nd	nd	nd	nd	nd	nd	nd
FeO	3.80	3.54	0.26	nd	nd	nd	nd	nd	nd	nd
MnO	0.07	0.10	0.04	0.05	0.06	0.08	0.05	0.08	0.04	0.09
MgO	3.46	3.80	0.18	5.21	4.92	6.56	3.64	3.09	1.78	6.64
CaO	0.64	3.44	0.11	2.3	3.88	3.88	0.84	5.05	0.16	4.82
Na_2O	0.36	1.73	1.77	2.32	3.7	2.56	2.03	5.03	2.68	2.15
K_2O	11.14	2.53	8.91	2.65	2.64	2.44	7.22	1.03	7.08	2.74
P_2O_5	0.16	0.09	0.01	0.12	0.12	0.15	0.12	0.07	0.1	0.14
SO_3	0.06	0.01	0.01	nd	nd	nd	nd	nd	nd	nd
CO_2	0.05	0.03	0.08	nd	nd	nd	nd	nd	nd	nd
H_2O^+	2.63	3.51	0.59	nd	nd	nd	nd	nd	nd	nd
S	0.0	0.0	0.0	0.18	0.2	0.11	0.15	0.05	0.06	0.14
TOTAL	99.56	99.83	99.47	99.75	99.59	99.48	99.37	99.66	99.55	99.93
LOI	2.26	3.15	0.64	3.79	3.74	3.26	2.54	2.36	1.59	3.34
Nd	-20	31	29	nd	nd	nd	nd	nd	nd	nd
Ce	-28	64	82	nd	nd	nd	nd	nd	nd	nd
La	-20	33	55	nd	nd	nd	nd	nd	nd	nd
Ba	2700	620	1620	286	306	433	2010	278	1220	664
Cr	11	60	9	nd	nd	nd	nd	nd	nd	nd
V	230	220	20	277	250	200	188	78	81	209
Sc	17	30	-9	nd	nd	nd	nd	nd	nd	nd
Th	16	14	26	nd	nd	nd	nd	nd	nd	nd
Sr	105	200	24	192	235	150	147	216	34	232
U	-10	-10	-10	3	5	5	13	6	9	5
Rb	320	79	220	155	160	130	212	40	218	117
Y	46	26	22	23	34	26	26	13	17	28
Zr	160	165	165	113	108	162	171	182	152	173
Nb	10	7	12	7	5	8.1	8.8	6	10.8	8
Mo	-5	-5	-5	nd	nd	nd	nd	nd	nd	nd
Co	23	26	-8	28	27	17	34	12	17	29
As	-20	-20	-20	nd	nd	nd	nd	nd	nd	nd
Bi	-5	-5	-5	nd	nd	nd	nd	nd	nd	nd
Ga	18	16	13	nd	nd	nd	nd	nd	nd	nd
Zn	50	76	18	58	60	60	52	23	32	49
W	-10	-10	-10	nd	nd	nd	nd	nd	nd	nd
Cu	77	-5	10	60	301	778	119	59	47	21
Ni	17	22	11	50	78	71	83	17	21	68
Sn	-9	-9	-9	nd	nd	nd	nd	nd	nd	nd
Pb	-10	-10	-10	2	2	2	-1.5	2	-1.5	2

Rock code 1 is feldspar-augite porphyritic andesite (minor clastic/breccia component)
Rock code 2 is medium-grained equigranular to weakly augite porphyritic diorite
Rock code 3 is porphyritic micromonzodioritic intrusions
Rock code 4 is acid (latite-?) andesite (quartz bearing)

Table 1

Compilation of whole rock analyses of the Thomas Creek intrusive complex and associated lavas (continued).

Sample No	18527	18528	18529	18530	18531	18532	18533	18534	18535	18536
Rock Code#	3	1	3	3	1	1	2	3	2	2
AMG mE	369800	370000	369800	369600	369600	369600	369600	369800	369400	370000
AMG mN	5285790	5285900	5285858	5285815	5285750	5285750	5285815	5285790	5286250	5285900
SiO_2	52.57	53.72	53.49	52.57	57.66	62.46	50.15	53	53.43	52.5
TiO_2	0.54	0.76	0.55	0.55	0.7	0.61	0.65	0.55	0.5	0.75
Al_2O_3	15.73	16.82	15.91	15.98	15.31	19.82	15.37	15.99	15.93	15.92
FeO*	11.86	10.94	11.06	11.82	6.95	2.37	11.66	12.24	5.62	13.22
Fe_2O_3	nd	nd	nd	nd	nd	nd	nd	nd	nd	nd
FeO	nd	nd	nd	nd	nd	nd	nd	nd	nd	nd
MnO	0.14	0.07	0.08	0.16	0.1	0.02	0.08	0.1	0.09	0.08
MgO	4.43	5.15	4.53	4.53	6.5	0.83	6	4.46	6.49	5.19
CaO	1.13	4.08	2.36	2.78	3.99	1.54	5.99	0.61	11.05	3.24
Na_2O	2.36	2.42	2.3	2.05	2.94	8.52	3.44	2.82	3.78	2.56
K_2O	6.4	2.02	5.07	4.85	1.29	1.94	2.05	5.69	1.07	1.38
P_2O_5	0.15	0.14	0.16	0.15	0.06	0.05	0.12	0.14	0.08	0.13
SO_3	nd	nd	nd	nd	nd	nd	nd	nd	nd	nd
CO_2	nd	nd	nd	nd	nd	nd	nd	nd	nd	nd
H_2O^+	nd	nd	nd	nd	nd	nd	nd	nd	nd	nd
S	0.16	0.08	0.16	0.14	0.04	0.23	0.22	0.21	0.02	0.14
TOTAL	99.19	100.30	99.70	99.86	99.65	99.94	99.64	99.52	100.20	99.88
LOI	2.56	2.95	2.96	3.11	3.38	1.52	2.84	2.56	1.56	3.44
Nd	nd	nd	nd	nd	nd	nd	nd	nd	nd	nd
Ce	nd	nd	nd	nd	nd	nd	nd	nd	nd	nd
La	nd	nd	nd	nd	nd	nd	nd	nd	nd	nd
Ba	1648	340	756	1212	221	307	502	1390	193	298
Cr	nd	nd	nd	nd	nd	nd	nd	nd	nd	nd
V	250	223	251	264	138	62	209	246	174	253
Sc	nd	nd	nd	nd	nd	nd	nd	nd	nd	nd
Th	nd	nd	nd	nd	nd	nd	nd	nd	nd	nd
Sr	119	225	102	140	192	131	155	86	346	172
U	5	2	6	6	2	82	4	7	-1.5	4
Rb	202	117	174	169	100	93	90	192	43	84
Y	18	14	18	15	15	30	20	17	24	19
Zr	83	109	85	83	156	151	84	82	59	112
Nb	6	6.2	5.5	6	5.3	8.7	4.5	5.1	2.9	6.1
Mo	nd	nd	nd	nd	nd	nd	nd	nd	nd	nd
Co	21	23	22	25	14	31	36	15	21	26
As	nd	nd	nd	nd	nd	nd	nd	nd	nd	nd
Bi	nd	nd	nd	nd	nd	nd	nd	nd	nd	nd
Ga	nd	nd	nd	nd	nd	nd	nd	nd	nd	nd
Zn	73	35	50	102	54	23	48	61	23	76
W	nd	nd	nd	nd	nd	nd	nd	nd	nd	nd
Cu	997	47	1124	340	264	268	401	1796	39	107
Ni	25	35	34	32	38	18	82	28	50	34
Sn	nd	nd	nd	nd	nd	nd	nd	nd	nd	nd
Pb	-1.5	4	-1.5	-1.5	3	10	-1.5	-1.5	3	2

Rock code 1 is feldspar-augite porphyritic andesite (minor clastic/breccia component)
Rock code 2 is medium-grained equigranular to weakly augite porphyritic diorite
Rock code 3 is porphyritic micromonzodioritic intrusions
Rock code 4 is acid (latite-?) andesite (quartz bearing)

Table 1

Compilation of whole-rock analyses of the Thomas Creek intrusive complex and associated lavas (continued).

Sample No	18537	18538	18539	NC462	NC385A	NC462A	NC058	NC085	NC150	NC065	NC098
Rock Code#	3	4	3	1	1	1	1	1	1	1	1
AMG mE	369800	369800	369800	368800	370300	368800	367300	367300	370000	366900	366800
AMG mN	5285858	5285790	5285790	5287800	5287000	5287800	5291900	5291800	5285500	5292300	5292300
SiO_2	59.04	58.77	54.86	55.2	55.9	51.8	62.1	62.2	63.4	64	64.2
TiO_2	0.69	0.59	0.63	0.55	0.61	0.59	0.66	0.66	0.55	0.54	0.53
Al_2O_3	17.47	15.63	15.03	15.5	14.9	13.9	16.6	16.9	15.6	15.8	16.2
FeO*	4.69	7.52	9.99	8.15	9	9	5.85	5.58	7.23	5.2	4.66
Fe_2O_3	nd	nd	nd	nd	nd	nd	nd	nd	nd	nd	nd
FeO	nd	nd	nd	nd	nd	nd	nd	nd	nd	nd	nd
MnO	0.09	0.06	0.09	0.21	0.07	0.28	0.08	0.11	0.07	0.06	0.07
MgO	3.97	3.31	5	5.05	6.06	8.9	2.45	2.1	2.71	1.9	1.97
CaO	1.34	1	2.48	7.58	5.97	9.24	4.86	5.54	1.89	4.47	4.87
Na_2O	3.92	1.43	2.34	4.93	2.79	2.64	3.21	2.94	3.6	3.38	3.35
K_2O	4.62	8.25	5.16	1.72	2.26	2.56	3.43	3.15	4.04	3.9	3.48
P_2O_5	0.08	0.12	0.13	0.11	0.11	0.1	0.15	0.16	0.12	0.16	0.13
SO_3	nd	nd	nd	nd	nd	nd	nd	nd	nd	nd	nd
CO_2	nd	nd	nd	nd	nd	nd	nd	nd	nd	nd	nd
H_2O^+	nd	nd	nd	nd	nd	nd	nd	nd	nd	nd	nd
S	0.13	0.08	0.19	nd	nd	nd	nd	nd	nd	nd	nd
TOTAL	99.51	99.64	99.43	100	100	100	100	100	100	100	100
LOI	3.08	2.13	2.61	3.79	1.45	2.37	1.7	2.44	2.56	1.49	1.6
Nd	nd	nd	nd	nd	nd	22.6	nd	nd	nd	nd	nd
Ce	nd	nd	nd	nd	nd	49.9	nd	nd	nd	nd	nd
La	nd	nd	nd	nd	nd	22.7	nd	nd	nd	nd	nd
Ba	1005	1968	1209	403	288	919	793	667	839	721	692
Cr	nd	nd	nd	70	213	342	29	30	39	19	16
V	192	206	205	225	185	211	152	132	169	125	130
Sc	nd	nd	nd	25	29	32	19	18	20	16	15
Th	nd	nd	nd	nd	nd	nd	nd	nd	nd	nd	nd
Sr	132	163	161	350	271	262	292	247	123	281	285
U	10	10	9	nd	nd	nd	nd	nd	nd	nd	nd
Rb	150	222	172	104	116	101	135	117	136	161	148
Y	19	24	38	20	28	18	34	28	39	29	29
Zr	184	173	147	74	145	55	199	184	161	204	199
Nb	10.6	8.6	7.6	4.1	7.3	3.2	14	13	8	13	14
Mo	nd	nd	nd	nd	nd	nd	nd	nd	nd	nd	nd
Co	12	14	22	nd	nd	nd	nd	nd	nd	nd	nd
As	nd	nd	nd	nd	nd	nd	nd	nd	nd	nd	nd
Bi	nd	nd	nd	nd	nd	nd	nd	nd	nd	nd	nd
Ga	nd	nd	nd	nd	nd	nd	nd	nd	nd	nd	nd
Zn	82	75	48	76	13	122	24	29	55	12	17
W	nd	nd	nd	nd	nd	nd	nd	nd	nd	nd	nd
Cu	765	524	1127	39	4	44	0	4	65	13	2
Ni	47	35	37	91	81	198	11	11	16	10	9
Sn	nd	nd	nd	nd	nd	nd	nd	nd	nd	nd	nd
Pb	-1.5	-1.5	-1.5	4	1.7	4	3	5	5	3	4

Rock code 1 is feldspar-augite porphyritic andesite (minor clastic/breccia component)
Rock code 2 is medium-grained equigranular to weakly augite porphyritic diorite
Rock code 3 is porphyritic micromonzodioritic intrusions
Rock code 4 is acid (latite-?) andesite (quartz bearing)

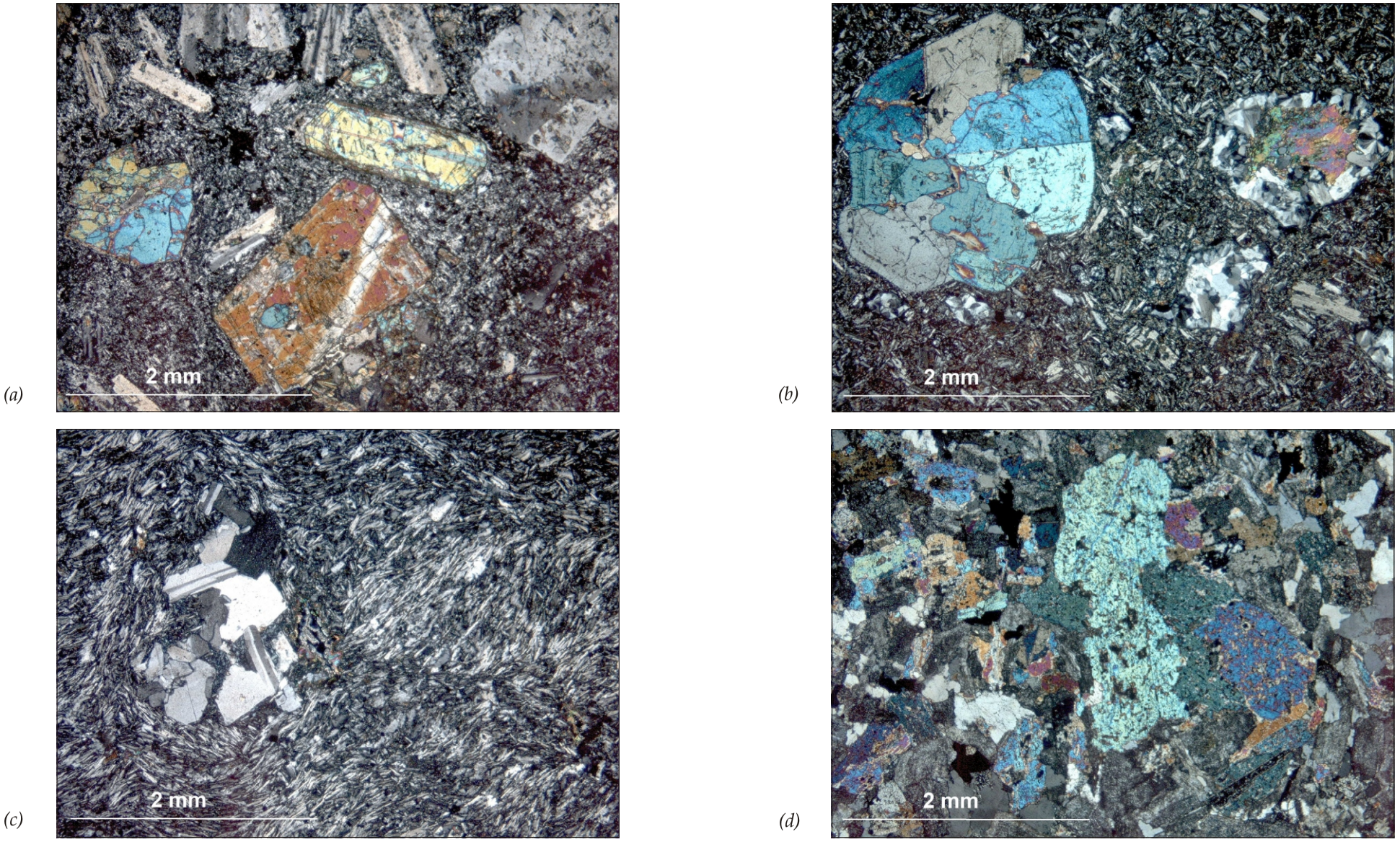

Figure 1

Photomicrographs (all with cross-polarised light) of representative analysed samples from the Thomas Creek area: (a) R002052, phenocryst-crowded clinopyroxene-plagioclase phyric andesite lava, Noddy Creek Volcanics; (b) R002056, amygdaloidal clinopyroxene-plagioclase phyric andesite lava with microcrystalline plagioclase-rich groundmass, Noddy Creek Volcanics; (c) R002054, feldspar-phyric fine-grained felsic lava with trachytic groundmass texture, Noddy Creek Volcanics; (d) R002058, diorite with interlocking medium-grained texture, Thomas Creek intrusive complex.

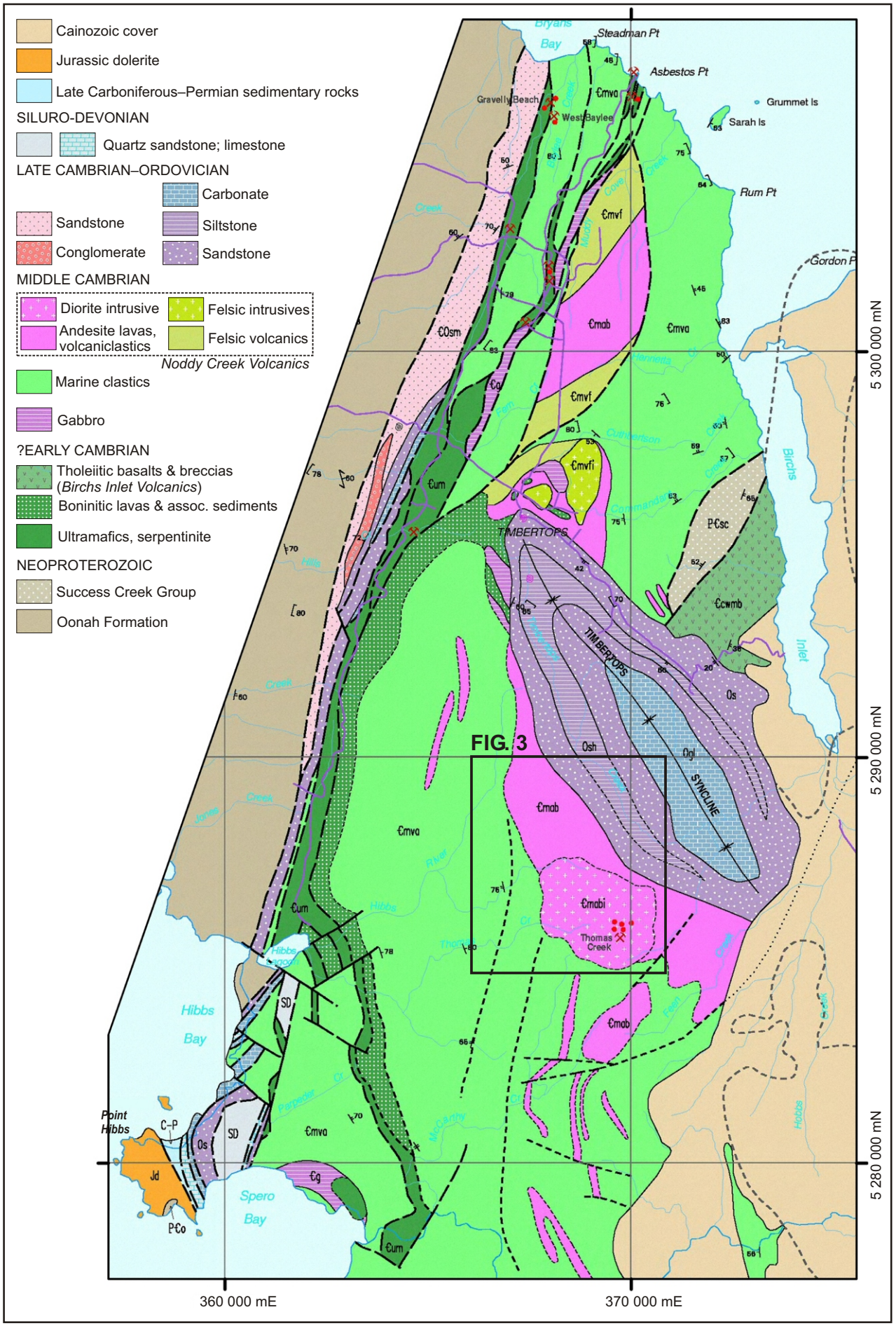

Figure 2

Regional setting of the Noddy Creek Volcanics, after Corbett (2002). Coverage of Figure 3 indicated.

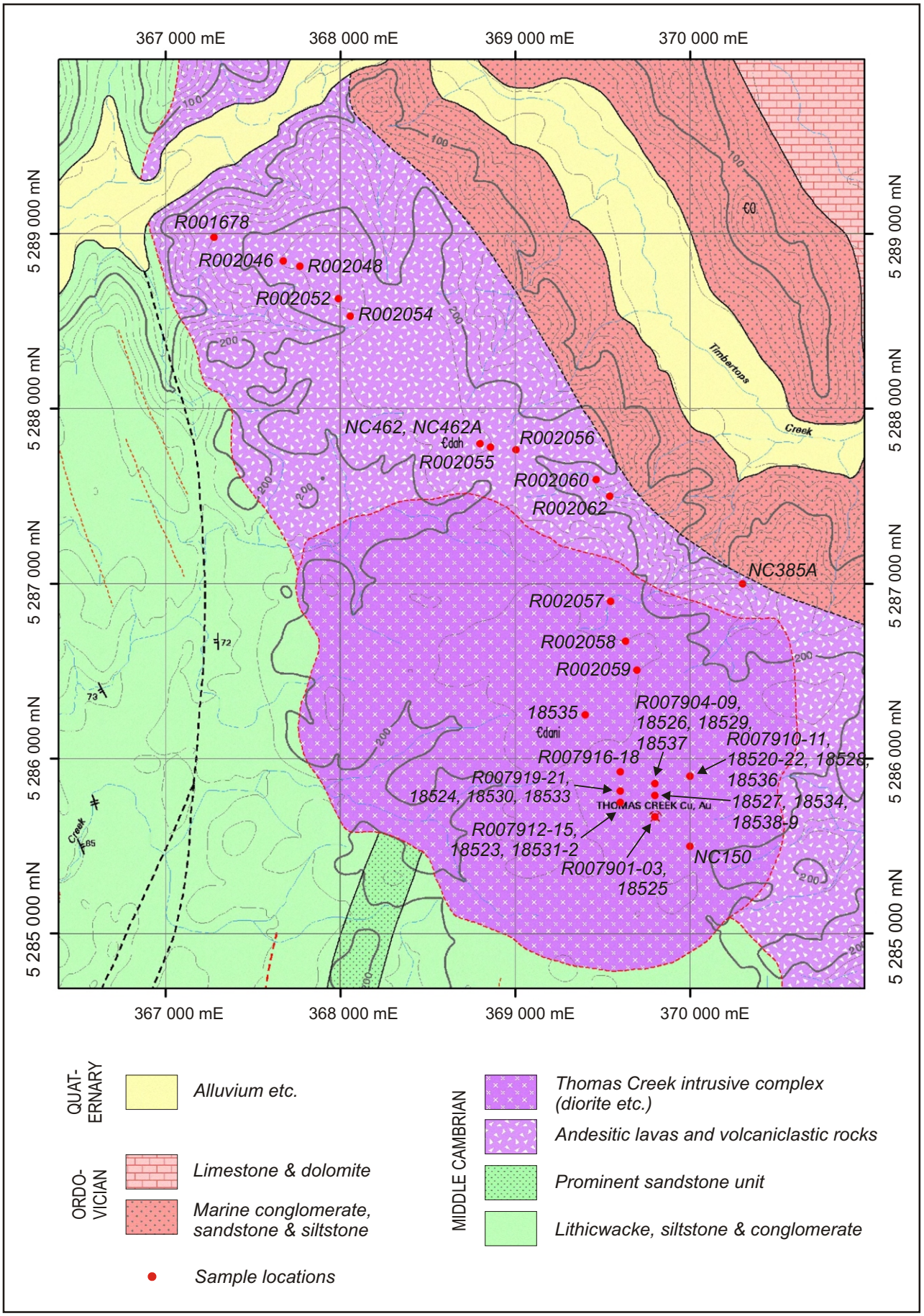

Figure 3

Geology of the Noddy Creek Volcanics in the Thomas Creek–Timbertops Creek area after Seymour and Green (2001), showing relationships between the Thomas Creek intrusive complex, adjacent andesitic lava-volcaniclastic sequence, and other sequences.

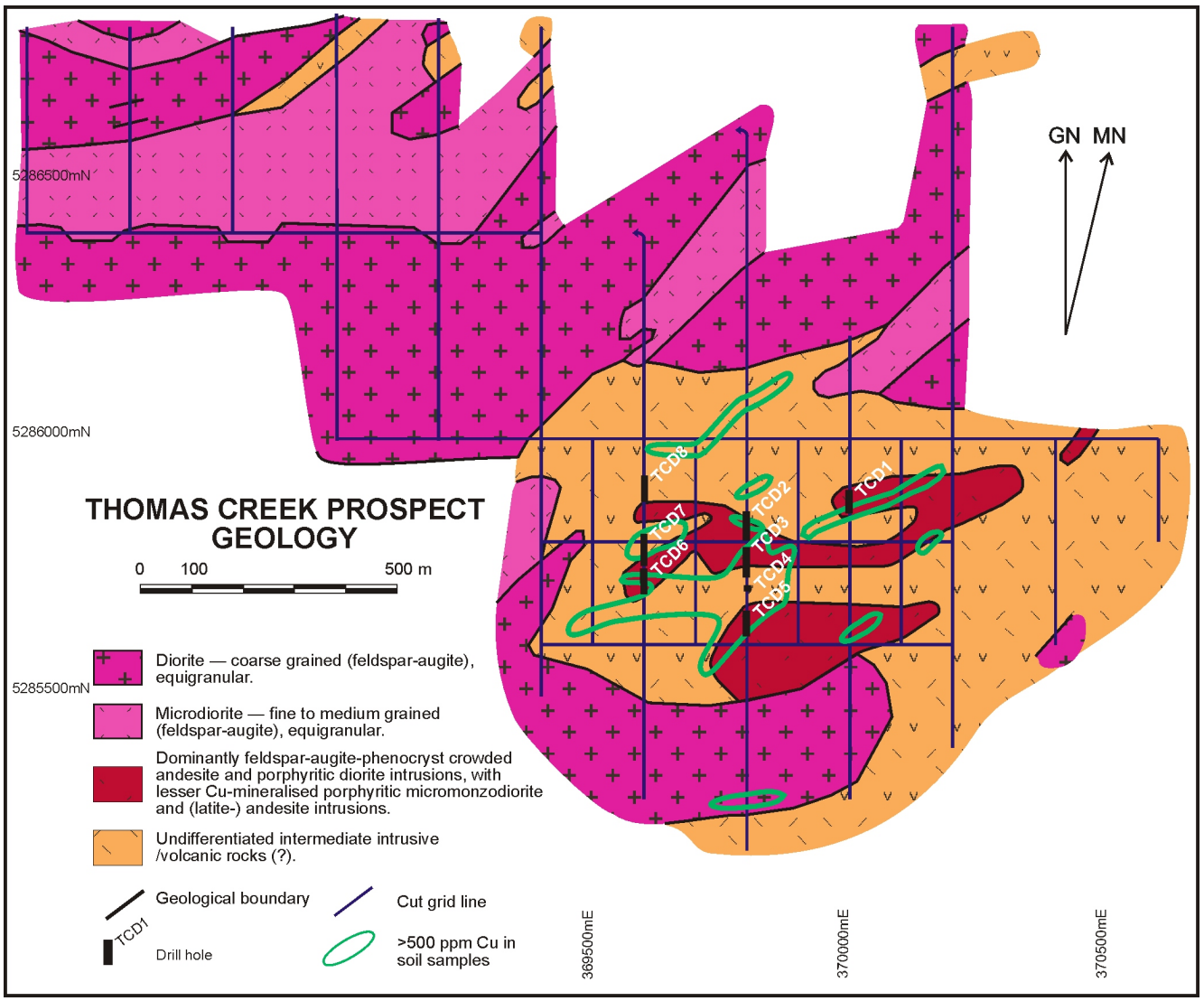

Figure 4

Detailed geology of the Thomas Creek prospect (from Reid, 2001), showing drill hole locations.

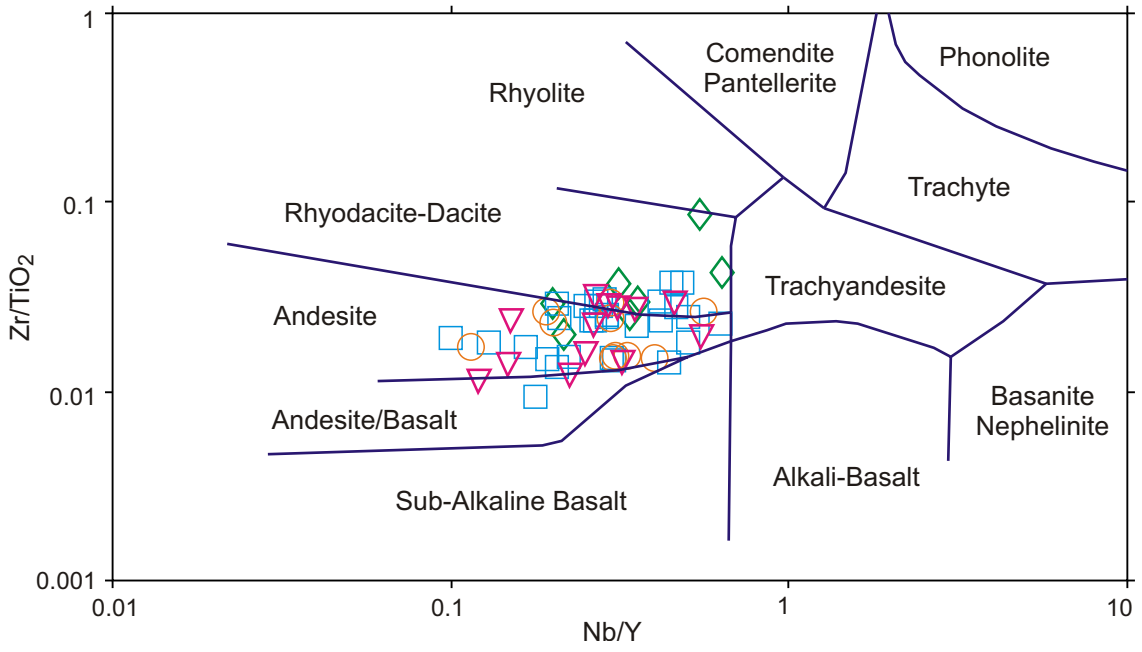

Figure 5

Nb/Y vs Zr/TiO_2 diagram for the Thomas Creek samples. Squares, triangles, circles and diamonds are for samples with rock codes 1 to 4 respectively. Fields from Winchester and Floyd (1977).

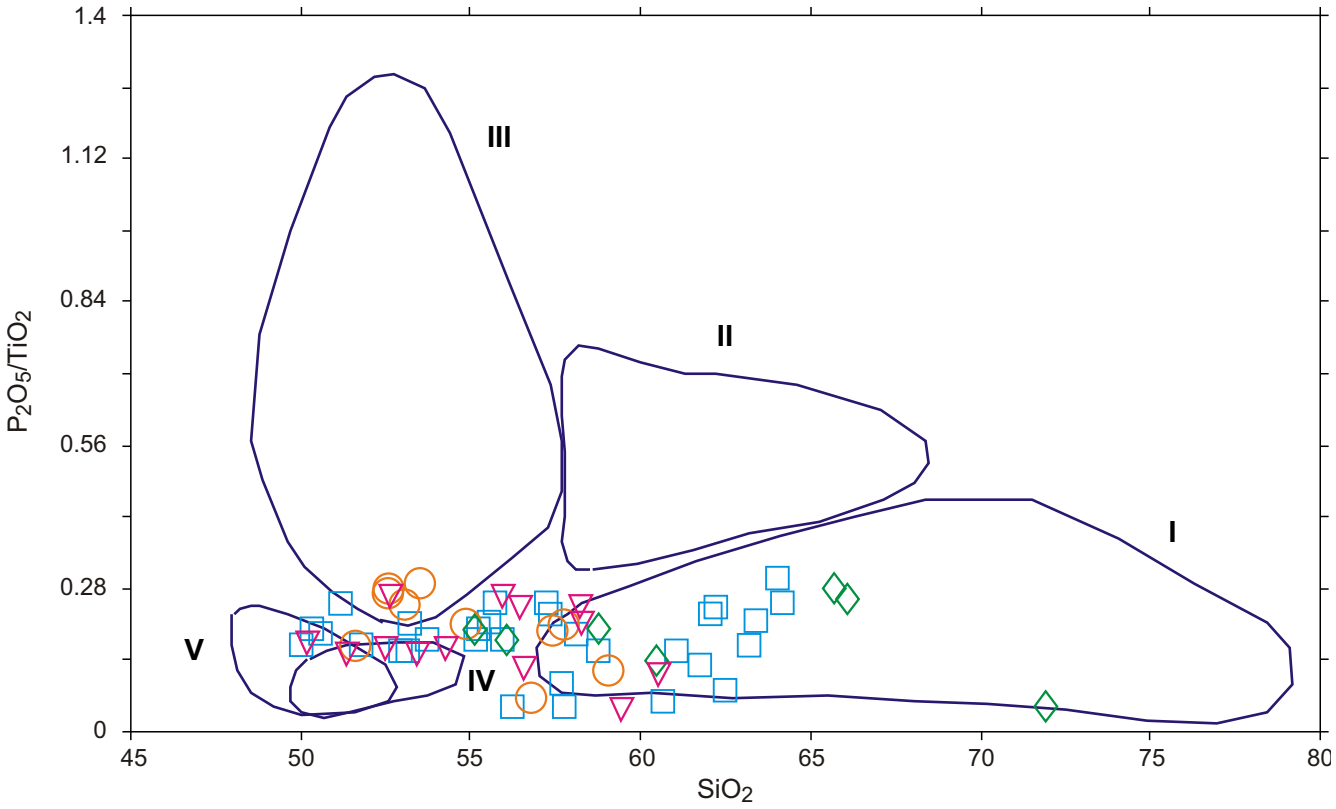

Figure 6

SiO_2 (wt%) vs P_2O_5/TiO_2 diagram for the Thomas Creek samples. Symbols as for Figure 5. Fields for MRV suites based on data in Crawford et al. *(1992).*

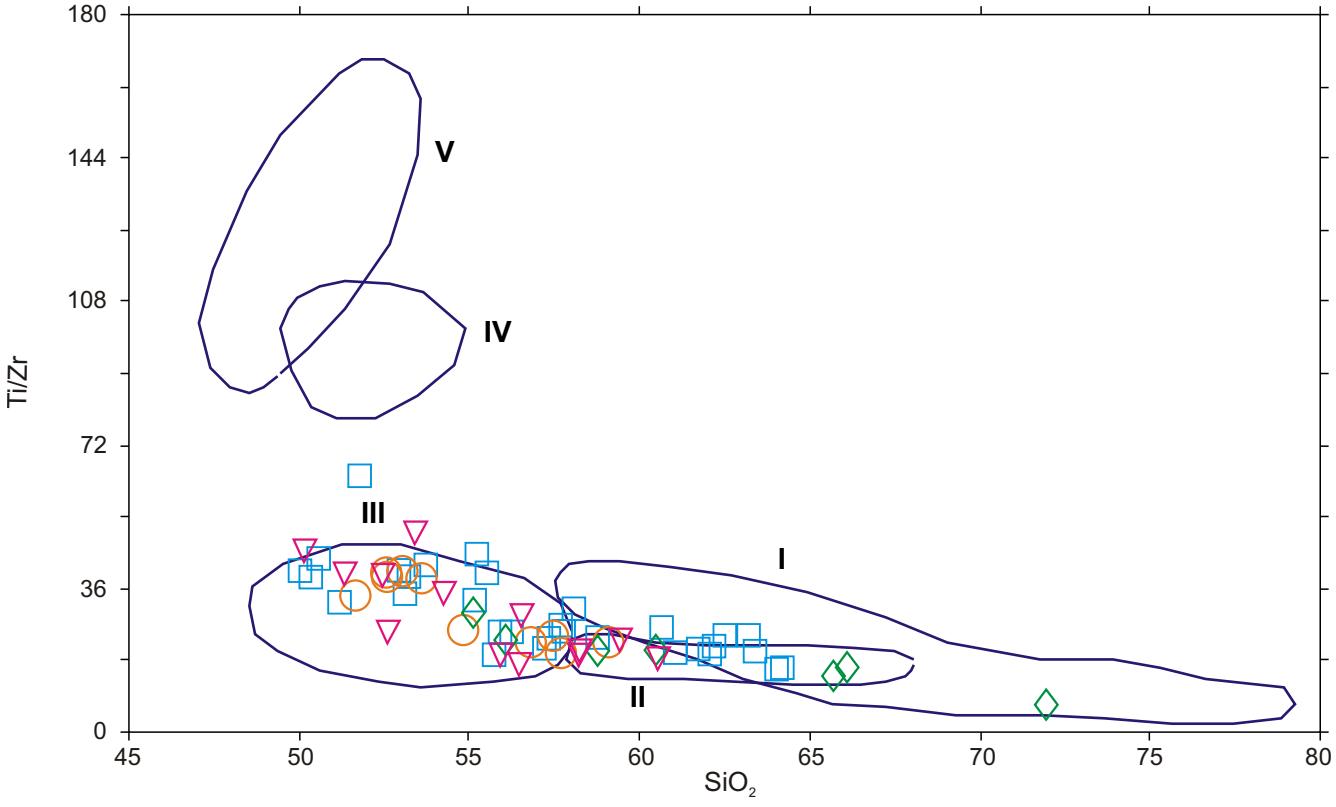

Figure 7

SiO_2 (wt%) vs Ti/Zr diagram for Thomas Creek samples. Symbols as for Figure 5. Fields for MRV suites based on data in Crawford et al. *(1992).*

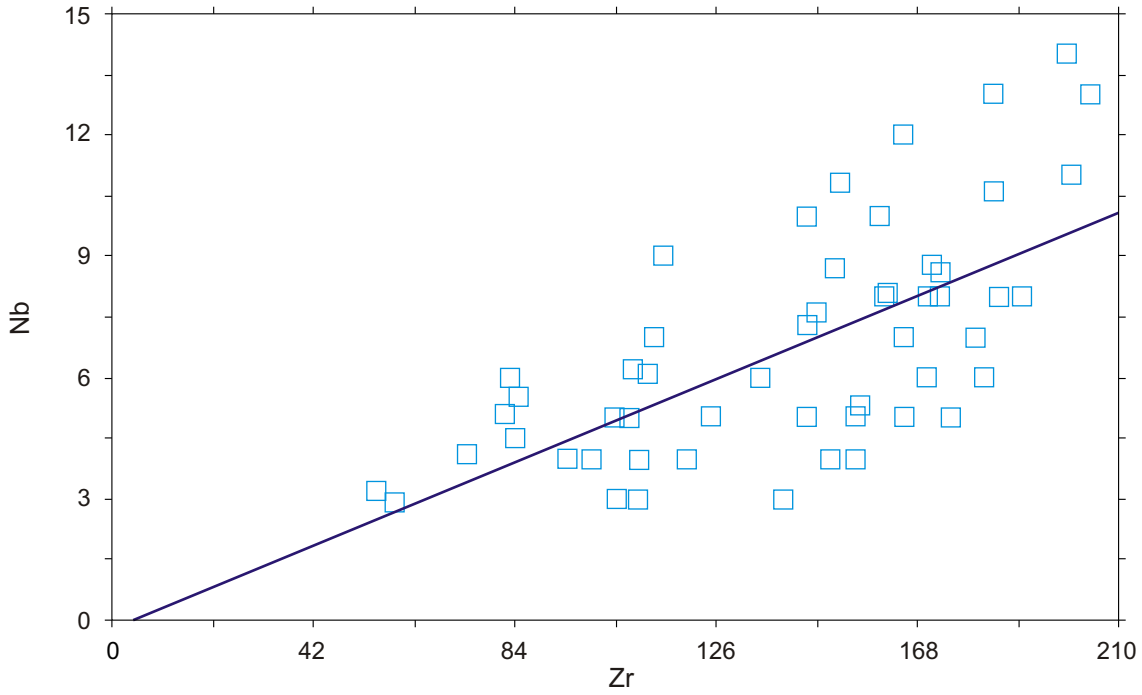

Figure 8

Zr (ppm) vs Nb (ppm) diagram for the Thomas Creek samples showing the best fit straight line. The line has a positive slope and intersects the Zr axis close to the origin, suggesting that Zr and Nb have almost equal levels of conservation (Stanley & Madeisky, 1993), and because of their incompatible character and relative immobile behaviour in hydrothermal solutions are probably both conserved.

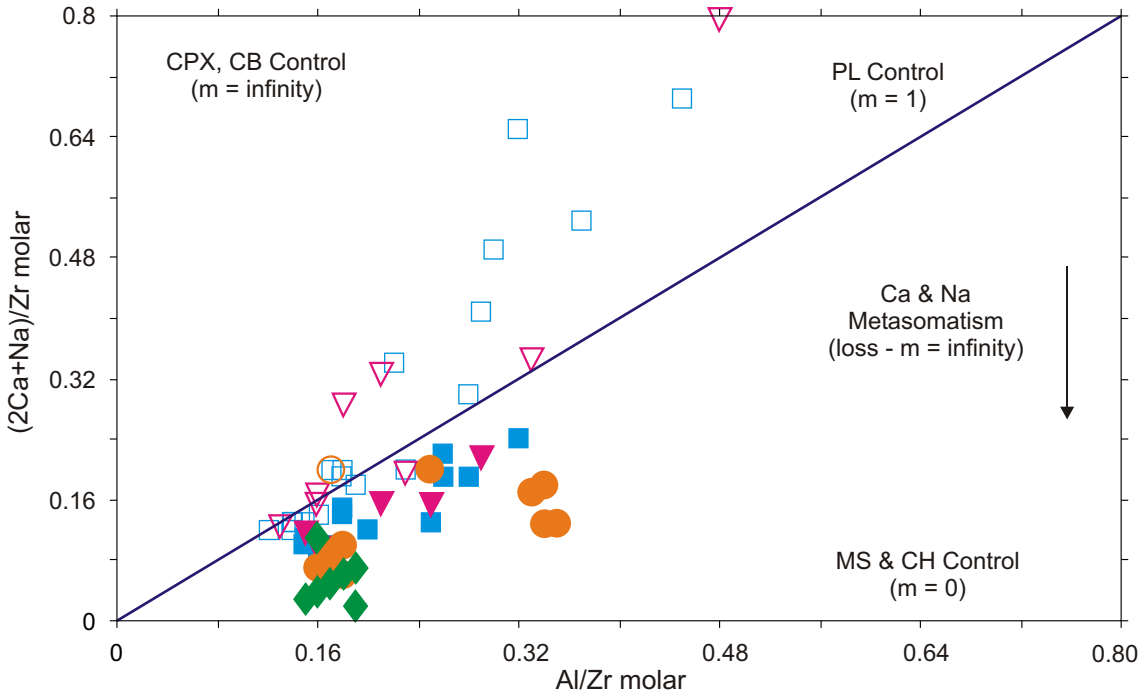

Figure 9

Al/Zr vs (2Ca + Na)/Zr PER assemblage test diagram showing the Thomas Creek samples. Addition of plagioclase (PL) and clinopyroxene (CPX) will displace rock compositions up and to the right along lines with slopes of unity and infinity, respectively. Addition of Ca-bearing carbonate veins (CB – calcite and dolomite) will displace rock compositions up along a line with infinite slope, and any Ca and Na metasomatic loss from these rocks will displace their compositions down along a line with infinite slope. Squares, triangles, circles and diamonds are for samples with rock codes 1 to 4 respectively and samples plotting significantly below the plagioclase control line (m = 1) have been indicated with filled symbols (i.e. samples with Al/(2Ca+Na) < 0.85) and are interpreted to be more hydrothermally altered. The trend away from the plagioclase control line for these samples may indicate metasomatic loss of Ca and Na and/or addition of muscovite (MS) and chlorite (CH).

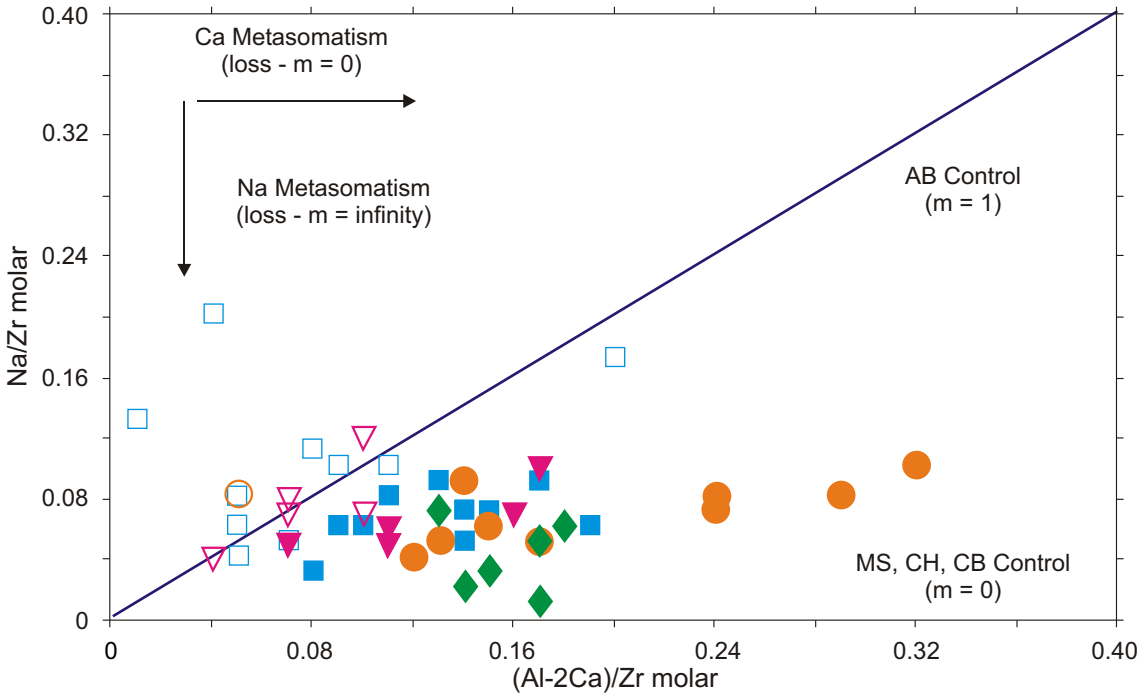

Figure 10

(Al-2Ca)/Zr vs Na/Zr PER assemblage test diagram showing the Thomas Creek samples. Symbols as for Figure 5. Addition of albite (AB) will displace rock compositions up and to the right along a line with unit slope. Addition of muscovite (MS) and chlorite (CH), and Ca-bearing carbonate veins (CB – calcite and dolomite), will displace rock compositions to the right and left along a line with zero slope, respectively. Less altered samples plot largely along the albite control line, confirming the control of plagioclase fractionation. More altered samples plot to the right of the albite control line along the muscovite and chlorite control lines (m = 0).

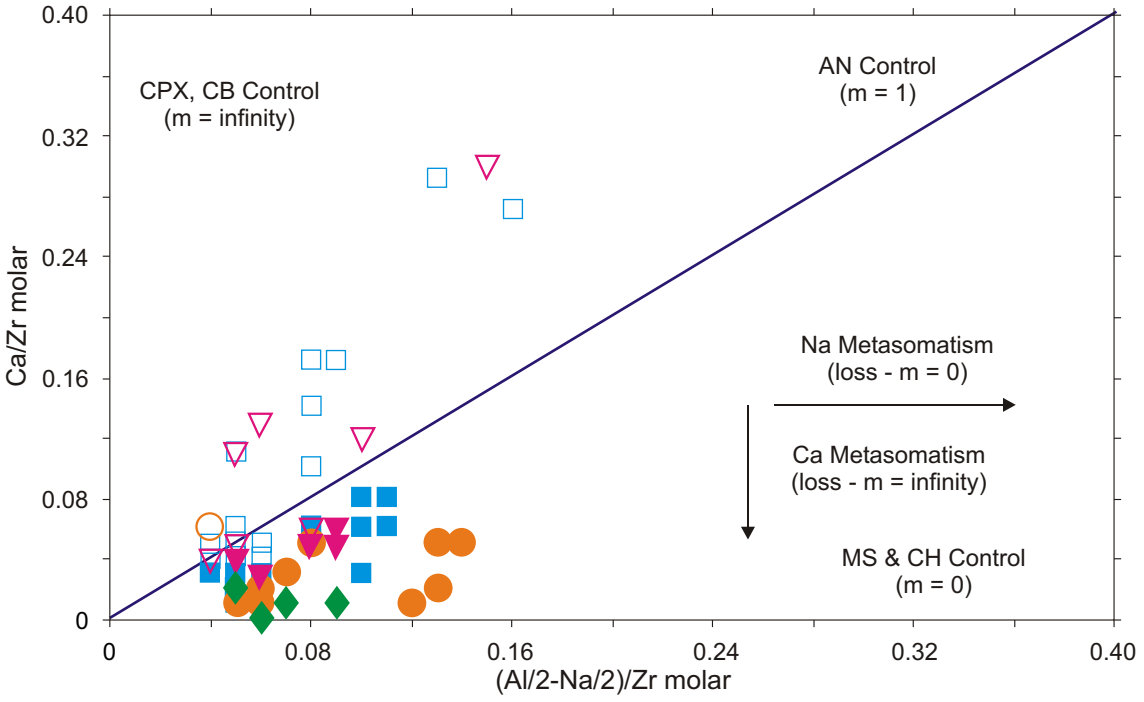

Figure 11

(Al/2-Na/2)/Zr vs Ca/Zr PER assemblage test diagram showing the Thomas Creek samples. Symbols as for Figure 5. Addition of anorthite (AN) will displace rock compositions up and to the right along a line with unit slope. Addition of muscovite (MS) and chlorite (CH), and Ca-bearing carbonate veins (CB – calcite and dolomite), will displace rock compositions up and to the right along lines with slopes of zero and infinity, respectively. Any Ca and metasomatic loss will displace rock compositions down and to the right along lines with slopes of infinity and zero, respectively. Less altered samples plot largely along a line that is steeper than the anorthite control line, confirming the control that both plagioclase and clinopyroxene have on the compositional variation. More altered samples plot to the right of the anorthite control line parallel to the muscovite and chlorite control lines (m = 0).

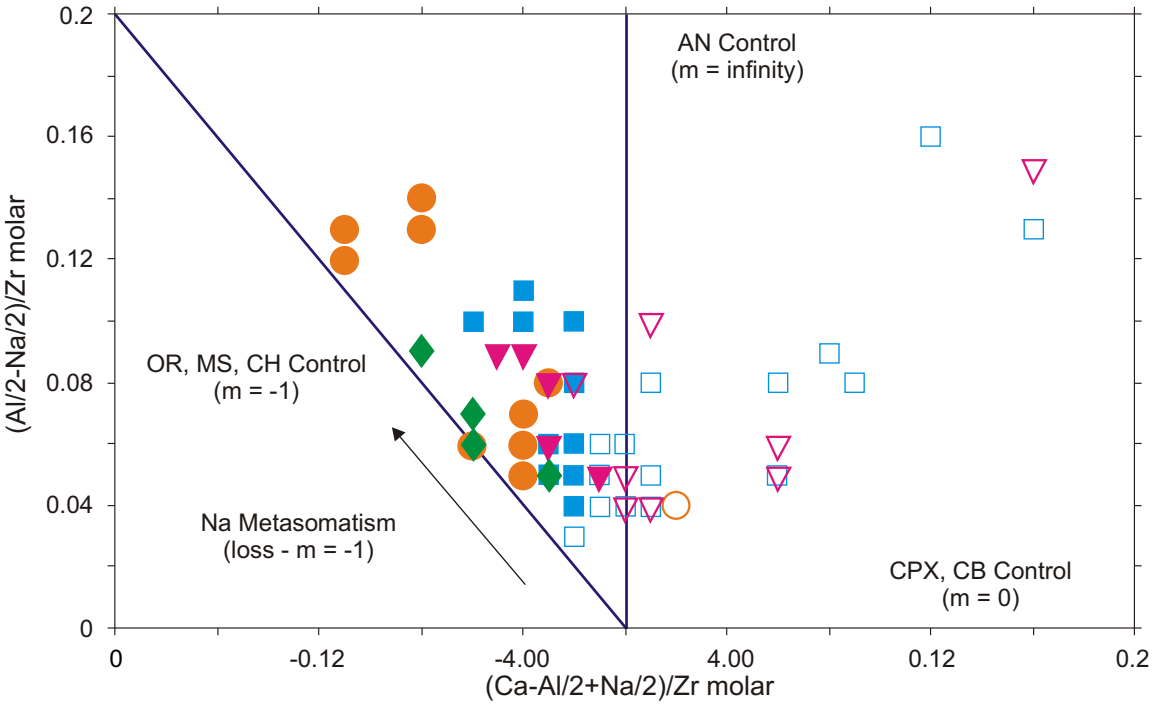

Figure 12

(Ca-Al/2+Na/2)/Zr vs (Al/2-Na/2)/Zr PER assemblage test diagram showing the Thomas Creek samples. Symbols as for Figure 5. Addition of anorthite (AN) and clinopyroxene (CPX) will displace rock compositions up and to the right along lines with slopes of infinity and zero, respectively. The less altered samples plot on a trend intermediate between these two lines indicating fractionation by anorthite and clinopyroxene. Addition of orthoclase (OR), muscovite (MS) and chlorite (CH) will displace rock compositions up and to the left on a line of negative unit slope. The more altered samples lie on trend with the same slope consistent with the addition of those minerals. This trend is also consistent with Na metasomatic loss.

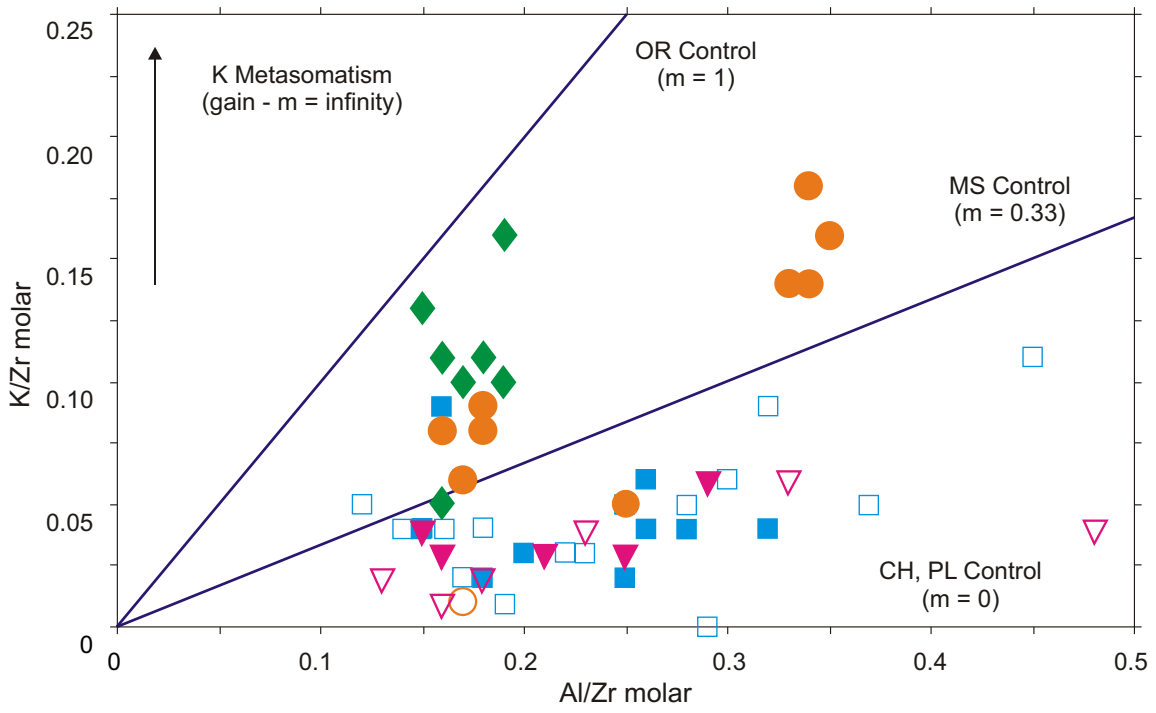

Figure 13

Al/Zr vs K/Zr PER assemblage test diagram showing the Thomas Creek samples. Symbols as for Figure 5. Addition of orthoclase (OR) will displace rock compositions along lines of unit slope, and addition of chlorite (CH) and plagioclase (PL) will displace rock compositions along a line of zero slope. Addition of muscovite (MS) will displace rock compositions up and to the right along a line of slope 1/3. K metasomatic gain will displace rock compositions up the diagram with a slope of infinity.

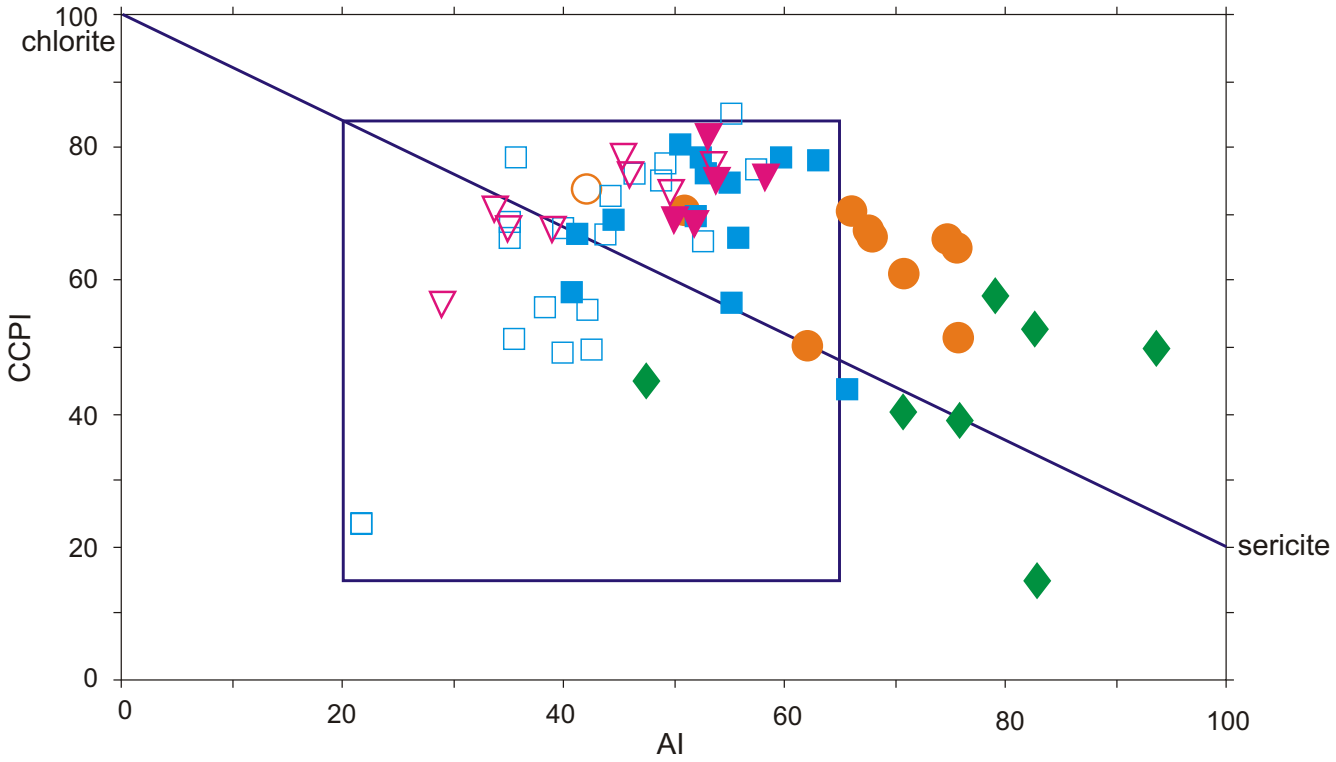

Figure 14

Thomas Creek area rocks displayed on the 'boxplot' diagram (Large, 1997) formed by plotting the Ishihawa alteration index (AI) (100(K_2O+MgO)/(K_2O+MgO+Na_2O+CaO) against the chlorite-carbonate-pyrite index (CCPI) (100(MgO+FeO)/(MgO+FeO+Na_2O+K_2O). Symbols as for Figure 5.